



Development and feasibility of quantitative dynamic cardiac imaging for mice using μ SPECT

M. A. Guerraty, MD, PhD,^a L. C. Johnson, PhD,^b E. Blankemeyer, BS,^b D. J. Rader, MD,^{c,d} S. C. Moore, PhD,^b and S. D. Metzler, PhD^b

^a Division of Cardiovascular Medicine, Department of Medicine, University of Pennsylvania, Philadelphia, PA

^b Department of Radiology, University of Pennsylvania, Philadelphia, PA

^c Division of Human Genetics and Translational Medicine, Department of Medicine, University of Pennsylvania, Philadelphia, PA

^d Department of Genetics, University of Pennsylvania, Philadelphia, PA

Received Sep 24, 2019; accepted Jan 23, 2020

doi:10.1007/s12350-020-02082-8

Background. Despite growing interest in coronary microvascular disease (CMVD), there is a dearth of mechanistic understanding. Mouse models offer opportunities to understand molecular processes in CMVD. We have sought to develop quantitative mouse imaging to assess coronary microvascular function.

Methods. We used ^{99m}Tc -sestamibi to measure myocardial blood flow in mice with MILabs U-SPECT⁺ system. We determined recovery and crosstalk coefficients, the influx rate constant from blood to myocardium (K_1), and, using microsphere perfusion, constraints on the extraction fraction curve. We used ^{99m}Tc and stannous pyrophosphate for red blood cell imaging to measure intramyocardial blood volume (IMBV) as an alternate measure of microvascular function.

Results. The recovery coefficients for myocardial tissue (R_T) and left ventricular arterial blood (R_A) were 0.81 ± 0.16 and 1.07 ± 0.12 , respectively. The assumption $R_T = 1 - \text{FBV}$ (fraction blood volume) does not hold in mice. Using a complete mixing matrix to fit a one-compartment model, we measured K_1 of $0.57 \pm 0.08 \text{ min}^{-1}$. Constraints on the extraction fraction curve for ^{99m}Tc -sestamibi in mice for best-fit Renkin–Crone parameters were $\alpha = 0.99$ and $\beta = 0.39$. Additionally, we found that wild-type mice increase their IMBV by $22.9 \pm 3.3\%$ under hyperemic conditions.

Conclusions. We have developed a framework for measuring K_1 and change in IMBV in mice, demonstrating non-invasive μ SPECT-based quantitative imaging of mouse microvascular function. (J Nucl Cardiol 2021;28:2647–56.)

Key Words: Microvascular dysfunction • SPECT • Myocardial blood flow • Small-animal imaging

Electronic supplementary material The online version of this article (<https://doi.org/10.1007/s12350-020-02082-8>) contains supplementary material, which is available to authorized users.

The authors of this article have provided a PowerPoint file, available for download at SpringerLink, which summarizes the contents of the paper and is free for re-use at meetings and presentations. Search for the article DOI on SpringerLink.com.

All editorial decisions for this article, including selection of reviewers and the final decision, were made by guest editor Stephan Nekolla, MD.

Reprint requests: M. A. Guerraty, MD, PhD, Division of Cardiovascular Medicine, Department of Medicine, University of Pennsylvania, 11-145 South Perelman Tower, 3400 Civic Center Blvd, Philadelphia, PA 19104; marie.guerraty@penmedicine.upenn.edu

1071-3581/\$34.00

Copyright © 2020 American Society of Nuclear Cardiology.

Abbreviations

CMVD	Coronary microvascular disease
FOV	Field of view
FBV	Fractional blood volume
IMBV	Intramyocardial blood volume
LV	Left ventricle
MBF	Myocardial blood flow
ROI	Region of interest
SPECT	Single-photon emission-computed tomography

See related editorial, pp. 2657–2659

INTRODUCTION

Coronary microvascular disease (CMVD), defined as disease of the coronary pre-arterioles, arterioles, and capillaries, is characterized by luminal obstruction, vascular rarefaction and remodeling, and endothelial and smooth muscle cell dysfunction.^{1,2} CMVD can result in ischemia or myocardial infarction with no obstructive coronary artery disease, and a growing body of work has shown the importance of the coronary microvasculature in affecting cardiac morbidity and mortality.^{3–5} Furthermore, there is evidence that CMVD may be involved in the pathogenesis of heart failure with preserved ejection fraction.^{6,7} Yet despite this growing awareness of the clinical significance of CMVD there is a dearth of basic mechanistic understanding of the pathophysiology and, therefore, there remain limited therapeutic options for CMVD.⁸

The microvasculature is highly dynamic and regulates myocardial blood flow (MBF) and flow reserve (MBFR) to meet cardiac metabolic demand. In the absence of epicardial coronary artery disease, MBFR is a direct measure of microvascular function. Though multiple cardiac imaging modalities, including MRI, PET, invasive doppler and echo, have been used to quantify MBF in patients, nuclear imaging with cardiac PET is the most clinically advanced modality for this purpose.⁹ These advances in imaging technologies have made it possible to measure and understand CMVD in a clinical population, yet our ability to evaluate microvascular function in pre-clinical models of CMVD is limited. Mouse models, in particular, have led to novel insights into mechanisms of cardiovascular disease due to their relative low cost and ease of genetic manipulation, which has recently been further revolutionized by the advent of CRISPR/Cas9, a novel genome editing technology.¹⁰ Understanding key molecular mechanisms to develop targeted therapies will require the use of mouse models, and in order to leverage mouse models to

study CVMD, it is critical to be able to measure microvascular function.

We have therefore sought to develop quantitative, non-invasive imaging in mice to measure microvascular function. Though several cardiac imaging modalities are available to measure microvascular function,^{11–13} echocardiography is either not quantitative (microbubble perfusion) or regionally restricted (Doppler coronary flow),¹⁴ and in comparison with MRI, μ SPECT is more quantitative and less expensive.¹⁴

In addition to MBF measurements, a novel index of microvascular function described by Mohy-Ud-Din et al. is based on measuring intramyocardial blood volume (IMBV) and change in IMBV with hyperemia as an elegant and alternative measure of microvascular function in canines.¹⁵ For both MBF and IMBV measurements, there are unique challenges to mouse imaging, including partial-volume effects from their small size and activity spillover, which call into question prior assumptions used for larger animals. In particular, human and large animal studies assume a relationship between the partial-volume effects in the myocardial tissue (R_T) and the fractional blood volume (FBV) from the arterial blood, which is typically defined as $R_T = 1 - \text{FBV}$.¹⁶ This is not established for small animals; therefore, we tested the validity of this assumption in mice. Similarly, the extraction fraction of ^{99m}Tc-sestamibi, the most commonly used cardiac SPECT tracer, is not known for mice. We used a μ SPECT system with multiple-pinhole collimation (U-SPECT⁺, MI Labs), which provides improved spatial resolution and high-sensitivity scans of mouse hearts, and reported our protocol, image acquisition, kinetic-modeling coefficients, and representative results. In this work, we adapt current methods, which are valid in larger animals, to the mouse scale.

MATERIALS AND METHODS

Dynamic Imaging Protocol for ^{99m}Tc-sestamibi

Mice (C57BL/6, Jackson Laboratories) ranging from 6 to 16 weeks and of both genders were used for imaging and protocol development with ^{99m}Tc-sestamibi ($n = 40$). Following sedation either with ketamine (100 mg/kg) and xylazine (10 mg/kg) or with isoflurane (3% initially then 1.5% during imaging), a tail-vein catheter was inserted and primed with ^{99m}Tc-sestamibi. Utilizing the small amount of radioactivity that reached the heart during catheter flushing, a scout scan was acquired and reconstructed to determine the precise bed position required to center the myocardium in the system's field of view (FOV). The FOV was approximately cylindrical with a 12 mm transverse diameter and a 7 mm axial length, the largest possible utilizing a single-bed position on the U-SPECT

system using the general-purpose mouse collimator, which has 0.35 mm spatial resolution.¹⁷ Animals were then imaged under basal conditions using a two-part sequence. First, dynamic data were acquired using a 4-minute list-mode acquisition for a single-bed position. 140 μ L of commercially obtained ^{99m}Tc-sestamibi (Nuclear Diagnostic Products, Cherry Hill, NJ) was injected via tail-vein catheter (3.79 ± 0.73 mCi) approximately 1 minute after starting the acquisition to ensure that the injection peak was fully captured. Following acquisition of the peak blood input-function data, five 1-minute frames were acquired using two-bed positions per frame to enlarge the axial FOV. Dynamic imaging data were obtained for 24 mice, and of these, 6 were used for microsphere experiments, whereas the remainder were sacrificed after imaging. To assess measured activity in the myocardium compared to ground truth and determine the recovery coefficient of myocardial tissue (R_T), a subset of imaged animals was sacrificed at the end of acquisitions, and the myocardium was excised, rinsed, assayed for radioactivity, and weighed. While establishing an optimal single-bed position protocol for dynamic imaging, there were mice with incomplete dynamic imaging data but with robust myocardial uptake in later frames ($n = 16$). For these mice, we were able to obtain R_T but not K_1 . All mouse experiments were approved by the University of Pennsylvania IACUC.

Image Processing and Kinetic Modeling

List-mode acquisitions from the early scans were retrospectively split into 10-second frames; two-bed position acquisitions from the later scans were automatically framed by the scanner. All frames were reconstructed using 0.2 mm cubic voxels with 10 iterations and 4 subsets and post-filtered (0.25 mm FWHM Gaussian filter). All reconstructions were used in conjunction with an activity-calibration factor, determined from a mouse-sized phantom using the same reconstruction parameters as the mice, such that the final image units were in μ Ci/mL.

In addition to by-frame reconstruction, a summed image of the last 5 min was reconstructed and used to draw regions of interest (ROIs) for data processing. ROIs were manually drawn for both the blood pool and the myocardial regions on the summed image and then applied to all by-frame data. This resulted in time-activity curves of the blood pool, $C_{BP}(t)$, and the myocardium, $C_{Myo}(t)$, for each mouse. Reconstructions were not corrected for either scatter or attenuation. We tested the effects of scatter and attenuation correction during both early dynamic acquisition and longer static acquisitions and found $< 8\%$ discrepancy between reconstructed images without corrections and with both scatter and attenuation correction for both the blood pool and LV ROIs. Since these corrections had only a small effect on reconstructed voxel values, and moreover since the activity-calibration factor had previously been determined using a mouse-size phantom reconstructed without scatter and attenuation corrections, we used uncorrected data for all analyses.

These time-activity curve data were used as inputs into our in-house kinetic-modeling software, in which no constraints were used between the spillover and recovery

coefficients, that is we did not assume $R_T = 1 - FBV$.¹⁸ To do this, we utilized the following mixing matrix:

$$\begin{pmatrix} C_{Myo}(t) \\ C_{BP}(t) \end{pmatrix} = \begin{pmatrix} R_T & F_A \\ F_T & R_A \end{pmatrix} \begin{pmatrix} C_T(t) \\ C_A(t) \end{pmatrix} \quad (1)$$

where C_T and C_A are the unknown time-activity curves for myocardial tissue and arterial blood pool, respectively, C_{Myo} and C_{BP} are the activity concentration values measured in the myocardial tissue ROI and in the arterial blood pool ROI, respectively, and the remaining four variables are the elements of the mixing matrix: (i) R_T is the recovery coefficient of the myocardium; (ii) F_A is the contribution of blood to the LV ROI including spillover from blood pool to LV and intravascular blood within the myocardium; (iii) R_A is the recovery coefficient of the blood pool; and (iv) F_T is the spillover from the LV myocardial tissue ROI into the blood pool ROI. Given the small scale of the mouse heart, we made no initial assumptions about the relationship between these parameters, but found theoretically that only one of F_A and R_A and only one of F_T and R_T needs to be known for a unique solution. We used experimentally determined population-averaged values for R_T and R_A , described below, and the standard 1-compartment kinetic model

$$\frac{dC_T(t)}{dt} = K_1 \cdot C_A(t) \quad (2)$$

to determine C_T , C_A , F_A , and F_T in conjunction with K_1 , the uptake rate constant from the blood into the myocardial tissue. We assume no tracer redistribution over the short time course of the experiment and thus $K_2 = 0$.

Red Blood Cell Imaging

Red blood cell imaging was performed on six mice and used to measure R_A , the spillover of arterial blood into the LV ROI, and to determine the intramyocardial blood volume (IMBV). For IMBV measurement, circulating red blood cells were labeled in vivo. Briefly, six mice were injected with 100 μ L of a commercial pyrophosphate (PYP) labeling kit (Pharmalucence, Billerica, MA) reconstituted in saline, and, following a 20-minute delay, injected with 4.45 ± 0.18 mCi of ^{99m}Tc-Pertechnatate. Two different sedation strategies were used since sedation can be a hyperemic stimulus for mice. For the first cohort ($n = 3$, mice 1 to 3), C57BL/6 male mice were initially sedated with ketamine and xylazine. During imaging, isoflurane was increased from 0% to 3% in a stepwise manner every 8 minutes through 0%, 1%, 1.25%, 1.5%, 1.75%, 2%, 2.5%, and 3% isoflurane, where doses of 1.25% or less should have minimal effect on the coronary microvasculature.¹⁹ 1-minute frames were obtained over 60 min. For the second cohort ($n = 3$, mice 4 to 6), mice were initially imaged with 2.5% isoflurane (10 minutes). Isoflurane was then decreased to 1.25% for basal IMBV measurements (15 minutes) and then increased to 3% to acquire hyperemic IMBV (10 minutes).

After acquisition, data were reconstructed into three separate frames, each approximately 10 to 15 minutes covering the three different isoflurane settings. The first 3 minutes after each dose change was excluded to allow time for the microvasculature to equilibrate. Following reconstruction (OSEM with 10 iterations and 4 subsets and 0.25 mm FWHM Gaussian post-filter), ROIs were drawn for both the LV myocardium and blood pool and the resulting activity concentration values were corrected for radioactive based on ROIs that were separately obtained from ^{99m}Tc -sestamibi imaging of littermates. To correct for biological decay, we used a linear correction to maintain blood pool activity constant and applied the same correction to the LV myocardial ROI.

To determine R_A , blood was drawn via retro-orbital bleeding, and radioactivity was measured. This value was activity decay-corrected to match the last image frame. The same ROIs were used as in the IMBV evaluation, and R_A was determined by the ratio of mean of the blood pool ROI to the activity concentration of the assayed drawn blood. This was calculated for the same six mice of the IMBV study.

Microsphere Validation Experiments

Myocardial perfusion experiments were successfully performed to measure resting myocardial blood flow in four of six mice. Briefly, mice were sedated with ketamine and xylazine and intubated. The abdominal aorta (AA) was cannulated with PE-10 tubing and the heart was exposed to allow for LV injection. A withdrawal pump (Harvard Apparatus) sampled central aortic blood at the rate of 60 $\mu\text{l}/\text{min}$ while 10 μm fluorescent microspheres (LifeSciences) were injected into the left ventricle. Following 2 minutes of circulation, the animal was sacrificed and the heart was collected and weighed. Tissue was digested using Solvable (PerkinElmer), and microspheres were extracted, washed, and quantified using an Accuri B6 Flow Cytometer (BD Biosciences). Myocardial blood flow was calculated as follows:

$$\text{MBF} = \text{Pump withdrawal rate} \times \frac{\# \text{microspheres in heart}}{\# \text{microspheres in blood}} \quad (3)$$

Statistical Analysis

All results are presented as mean \pm standard deviation. Outliers were detected using Robust regression and Outlier method with Q of 1%.²⁰ One-sample T test was used to compare the sum of R_T and F_A with a mean of 1, and linear regression modeling was performed using Prism 8.2.0. The paired values for K_1 and MBF were plotted and fitted to the form of the Renkin–Crone model, found below in (4).^{21,22} The χ^2 match between the analytic form and the data was minimized. A Monte Carlo procedure generated 10,000 replicate data sets. For each actual data pair, a simulated pair was inserted into each replicate set after it was generated following a Gaussian distribution with the same means and standard deviations as the empiric data, 0.083 min^{-1} and 2.56 $\text{ml}/\text{g}/\text{min}$ for K_1 and MBF, respectively. These replicate sets were also fit to determine the minimum χ^2 and the $\Delta\chi^2$ for the fitted Renkin–Crone parameters. From this $\Delta\chi^2$ distribution, the 50%

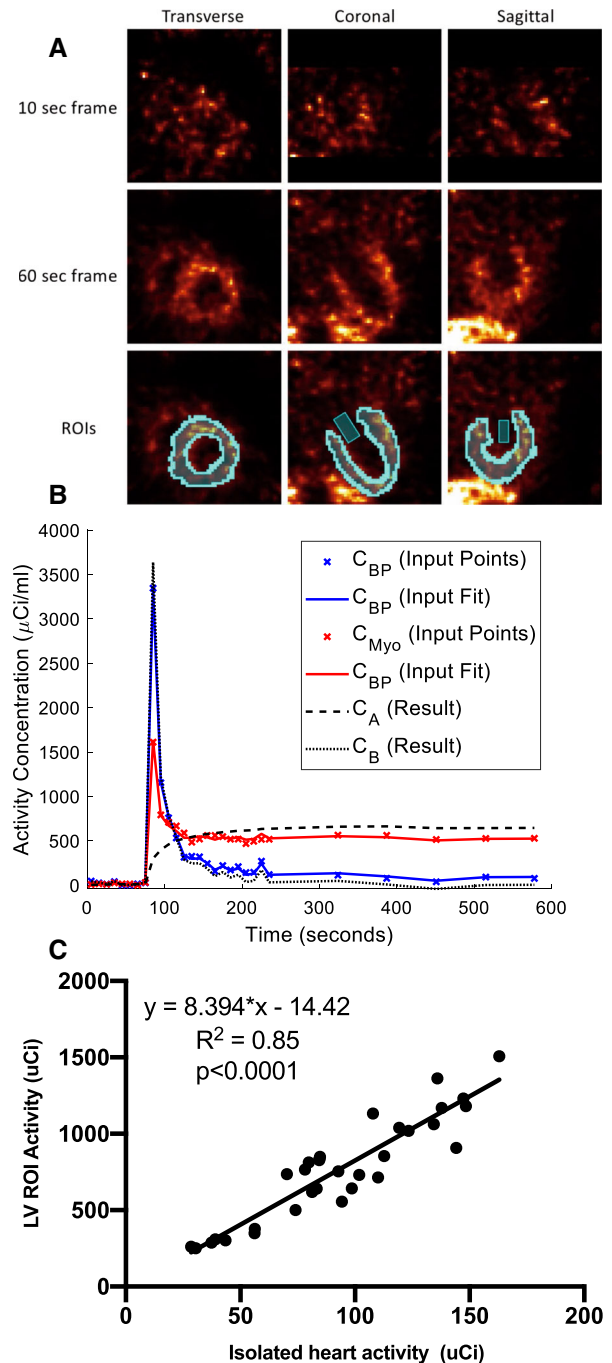


Figure 1. A Representative images acquired using 10-second and 60-second frames after injection of ^{99m}Tc -sestamibi illustrate high resolution of uSPECT system and the ability to define blood pool (small rectangle) and LV myocardial (thick blue outline) ROIs. B Activity concentration plotted over time shows the activity in the blood pool initially increased and then quickly decreased to near zero, with an increase in LV activity over time. C There is a strong correlation between the activity of the LV ROI as determined by uSPECT and isolated heart activity measured in a well-counter.

and 90% confidence levels were estimated (i.e., what values for contain the true model parameters 50% and 90% of the time, respectively). Those $\Delta\chi^2$ values were used to generate the contours of the allowable space for the model Renkin–Crone parameters in mice.

RESULTS

Dynamic Mouse Imaging

Using the U-SPECT system, we were able to obtain high-resolution dynamic blood pool and LV myocardial ROI measurements. Representative ROIs obtained early (10-second frames) and late (1-minute frames) following injection are shown in Figure 1A. The resulting time-activity curves for both blood pool and LV ROIs were captured using 10-second frames and show a brisk arterial input function and gradual accumulation of radiotracer in the LV ROI (Figure 1B). There is high correlation between LV myocardial activity as quantified by imaging and the activity in isolated heart tissue quantified using a well-counter (Figure 1C).

Determination of Recovery Coefficients

To determine K_1 , the uptake rate constant from the blood into the myocardial tissue, we used a 1-

compartment model in conjunction with the mixing matrix defined in Eq. 1. As mentioned before, that fit requires that one of the two elements in each column of the mixing matrix is known in advance to achieve a unique solution for K_1 .

To measure R_T for a range of mouse sizes (18–25 g), the heart was excised immediately after imaging, and the activity per mg of tissue was measured and compared to the activity concentration obtained from the second half of the dynamic protocol, binned into a single 5-minute frame. We found that our recovery coefficient was higher for larger hearts, and the mean value of R_T was 0.81 ± 0.16 (Figure 2A, $n = 34$). We found a modest and statistically insignificant relationship between heart mass and body weight (Pearson correlation 0.46, $p = .06$), and no association between R_T and body mass (Pearson correlation -0.03 , $p = .93$), (Figure 2B). To measure R_A , we measured the activity of ^{99m}Tc -tagged red blood cells in the blood pool and LV ROIs using ROIs that were separately obtained from ^{99m}Tc -sestamibi imaging of littermates. This was compared with blood sampled immediately after imaging to determine that R_A was 1.07 ± 0.12 (Table 1).

With these measured R_A and R_T values, the spillover coefficients F_A and F_T were fitted (along with K_1) using Eq. 1. For larger animals, the assumption that $R_T = 1 - \text{FBV}$, is often used to simplify Eq. 1. We

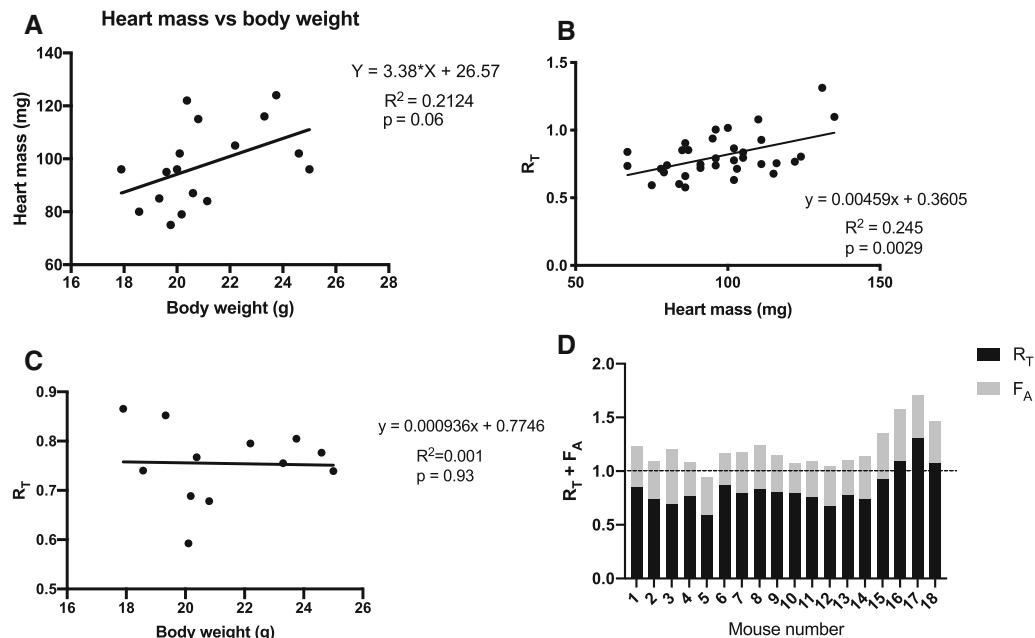


Figure 2. **A** Heart mass versus body weight for mice that were imaged shows a wide range of mouse body and heart sizes. **B** Recovery coefficient (R_T) increases with increases in heart size; however, R_T is not positively associated with body weight (**C**), where p-values represent significance relative to no correlation. **C** The sum of the R_T and F_A measured in 18 mice was greater than 1 (mean 1.25 ± 0.20 , $p < .0001$).

Table 1. Blood pool ROI activity was compared to the activity of isolated blood to determine R_A

Mouse	ROI blood pool activity concentration (μ Ci/ml)	Isolated blood-activity concentration (μ Ci/ml)	R_A
1	628.8	638.5	0.98
2	681.8	670.0	1.02
3	617.8	620.0	1.00
4	597.0	518.0	1.15
5	437.6	338.3	1.29
6	371.5	373.0	0.99
Mean \pm SD	555.7 \pm 122.2	526.3 \pm 142.1	1.07 \pm 0.12

calculated the sum of measured R_T and the fitted F_A values for 18 mice and found that mean sum was 1.25 ± 0.20 , and not equal to 1 ($p < .0001$, Fig. 2D), suggesting that this assumption does not hold in mice.

We next determined $K1$ and obtained a range of $K1$ of $0.58 \pm 0.08 \text{ min}^{-1}$ using population-averaged R_T values (Figure 3A). $K1$ obtained using individual R_T values was similar to $0.51 \pm 0.11 \text{ min}^{-1}$ with high correlation between $K1$ values obtained using a population-averaged R_T and individual R_T (Pearson correlation 0.8244, $p < .0001$). To determine constraints on the extraction fraction curve for ^{99m}Tc -sestamibi in mice in vivo, we used microsphere perfusion experiments to measure absolute myocardial blood flow in four mice that were previously imaged with the dynamic protocol. The relationship between MBF and $K1$ is given by the Renkin–Crone model, which is a 1-compartment model that describes transport of the radiotracer from the blood pool to the tissue with no redistribution [16,21,22]

$$K1 = \text{MBF} \times \left(1 - \alpha e^{-\frac{\beta}{\text{MBF}}}\right) \quad (4)$$

where α and β are the Renkin–Crone extraction fraction parameters and α is sometimes denoted ‘‘a.’’¹⁶ More specifically, α and β describe the relationship between MBF and the transport of the radiotracer across the capillary wall over a given surface area.¹⁶ Based on the fit in Figure 3B, we determined $\alpha = 0.99$ and $\beta = 0.39$ in mice, which are in line with previously published values.²³ Figure 3C shows the allowable region for α and β at 50% and 90% confidence levels.

We next evaluated change in IMBV as an alternative measure of microvascular function. Intramyocardial and blood pool activity of ^{99m}Tc -tagged red blood cells in mice at basal and hyperemic conditions were measured. Since sedation is known to affect the degree of hyperemia, we used two complementary approaches.

Three mice were sedated with ketamine and xylazine, which do not affect MBF,¹⁹ and then treated with increasing doses of isoflurane. A representative example shows an increase in activity concentration in the LV myocardium ROI with increasing doses of isoflurane (Figure 4A). A second cohort of three mice was sedated with only isoflurane, initially 2.5%, then 1.25%, and finally 3% (Figure 4B). In both cases, 3% isoflurane was used to induce hyperemia and this was compared to a basal state of ketamine–xylazine sedation only (mice 1–3) or 1.25% isoflurane sedation (mice 4–6). Both cohorts displayed a similar degree of increase of IMBV in response to hyperemia, suggesting that wild-type adult mice increase IMBV $22.9 \pm 3.3\%$ in response to hyperemia (Table 2).

DISCUSSION

Mice present unique opportunities for molecular and genetic studies and have been the model organism of choice for cardiovascular research over the past two decades.²⁴ With growing interest in CMVD,⁸ the ability to easily and non-invasively assess microvascular function in a pre-clinical model is crucial to understanding the pathophysiology and developing potential therapies. Yet there are challenges unique to mouse imaging, which must first be addressed. We developed and validated protocols for dynamic cardiac imaging of mice using μ SPECT and established recovery coefficients. Additionally, our results show the need to fully fit the mixing matrix to minimize assumptions that do not hold for small animals.

Using μ SPECT with pinhole collimation, which has superior resolution compared to μ PET, we were able to measure time-activity curves of both the blood pool and LV myocardium. We measured R_T and found that though it correlates with heart mass, it does not correlate with body weight. $K1$ obtained using population-

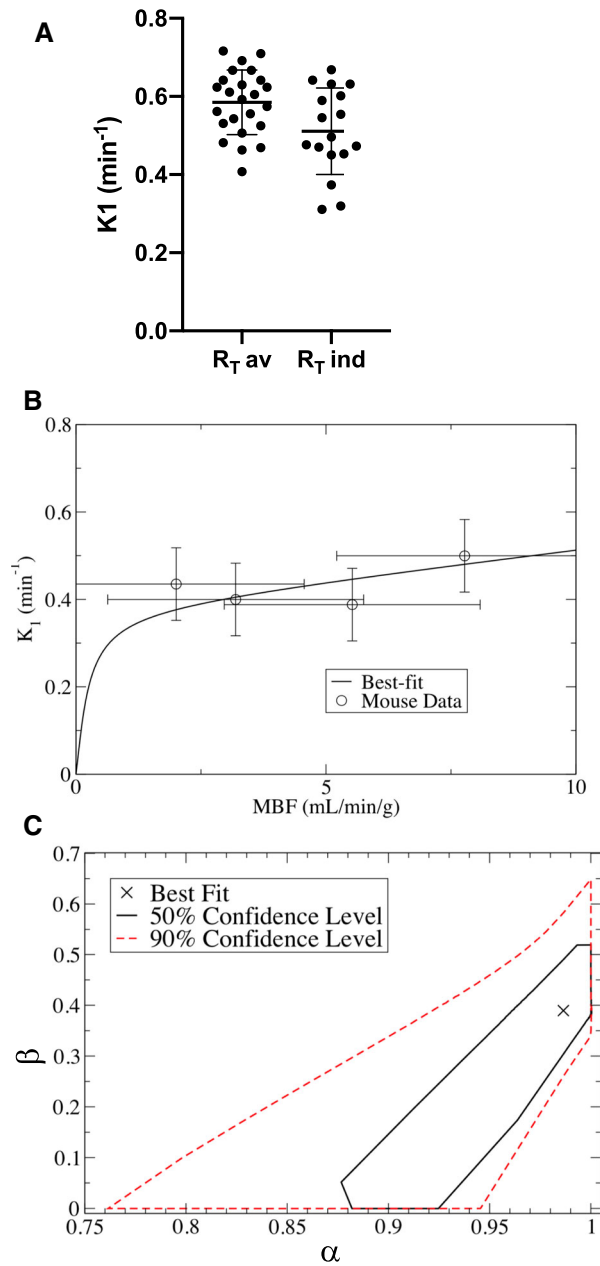


Figure 3. **A** Using population-averaged R_A and both population-averaged and individual R_T , K_1 was obtained under resting conditions. **B** To set constraints on the extraction fraction, absolute MBF was measured using fluorescent microsphere perfusion. **C** Based on microsphere measurements of MBF, the best fit for α and β was 0.99 and 0.39, respectively.

averaged R_T is similar to K_1 obtained using individually measured R_T . Together, these support the use of a population-averaged R_T in mice. We also measured R_A to be 1.07 ± 0.12 . We determined that, due to the small size of mouse hearts, the assumption often used in

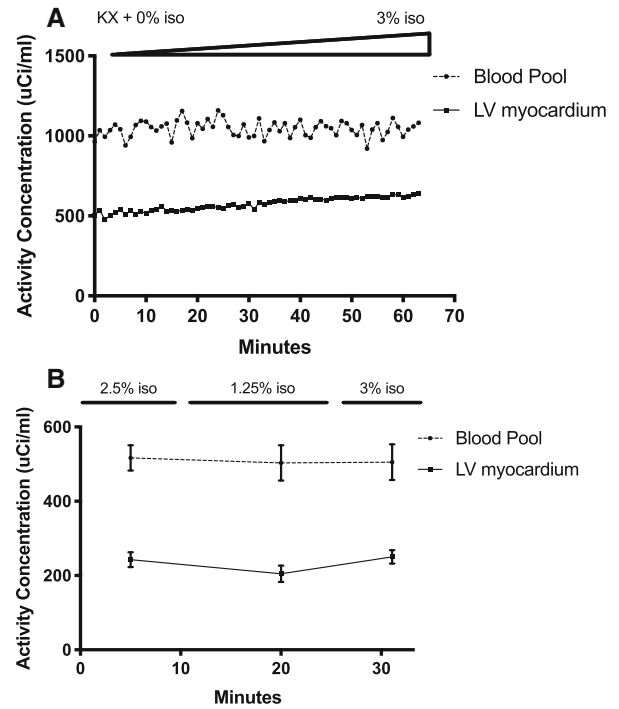


Figure 4. **A** Representative blood pool and LV myocardial ROI values with activity concentration corrected for biological and radioactive decay during the duration of the whole scan for IMBV imaging of Mouse 2. Mice were sedated with ketamine and xylazine (KX) and isoflurane was increased from 0% at $t = 0$ (basal state) to 3% at $t = 52$ min (hyperemic state). **B** Blood pool and LV myocardial ROI values with activity concentration corrected for biological and radioactive decay for IMBV imaging of mice 4-6, which were sedated with only isoflurane.

humans and larger animals ($RC = 1 - FBV$) does not hold for small mice, and a full matrix of mixing parameters is needed. Though this is likely due to limited spatial resolution, a second potential reason for this may be the increased flow rate and IMBV in mice which adds a second source of blood-activity contribution to the LV ROI. Of note, our model assumes that there is no redistribution of ^{99m}Tc -sestamibi. Though ^{99m}Tc -sestamibi redistribution has been noted in larger animals,^{25,26} it is likely not contributing significantly during early dynamic imaging protocol in the absence of coronary stenoses. However, this will be an important consideration in imaging mouse models of coronary artery disease.

MBF is known to be higher in mice than in humans,^{9,13} and the extraction fraction of ^{99m}Tc -sestamibi is limited at high flow rates.¹⁶ However, there are only limited data about the extraction fraction of ^{99m}Tc -sestamibi in vivo. Leppo and Meerdink reported ex vivo

Table 2. The difference in IMBV between basal resting and hyperemic (3% isoflurane) conditions reflects microvascular function in normal wild-type mice

Mouse	ROI basal activity concentration (μ Ci/ml)	ROI hyperemic activity concentration (μ Ci/ml)	% increase
1	509.0	625.5	22.9
2	402.2	497.5	23.7
3	304.1	366.0	20.3
4	196.6	248.3	26.3
5	190.2	238.2	25.2
6	229.6	269.2	17.2
Mean \pm SD	305.8 \pm 127.8	374.1 \pm 157.3	22.6 \pm 3.4

values for rabbit hearts,²³ and Mousa et al. measured the extraction fraction of ^{99m}Tc -sestamibi in vivo in pigs.²⁷ These extraction curves are quite different, such that the shoulder of the extraction fraction curve where extraction and MBF transition from linear to exponential occurs at MBF of 0.5 ml/min/g in the former and close to 3.6 ml/min/g in the latter. These discrepancies may be due to different experimental designs or may be species-specific, and it has not been determined how these findings translate to mouse imaging. To determine constraints on the extraction fraction of ^{99m}Tc -sestamibi in mice, microsphere perfusion experiments were performed to measure MBF in vivo. In these experiments, we measured MBF of 5.4 ± 2.7 ml/min/g, which is consistent with both the range and variability that has been described for mice using other imaging modalities.¹³ This constrains the extraction curve to be closer to that of Leppo and Meerdink for mice.

Based on the results of the fit in Figure 3B, it is possible that ^{99m}Tc -Sestamibi may be a useful tracer for measuring disease processes that reduce resting MBF to less than 2 ml/g/min. Future studies in mouse models of CMVD will determine the sensitivity of ^{99m}Tc -sestamibi to detect decreases in MBF. On the other hand, MBF imaging of hyperemic blood flow in mice, where the true MBF will be substantially higher than 2 ml/g/min, is likely to require using a tracer with a higher extraction fraction for reliable conversion back to MBF. Thallium-201 may be an alternative, given its improved extraction at higher flow rates. As an additional metric for quantifying microvascular function in mice, we extended earlier works by others in large animals to show that mice increase their IMBV by $22.6 \pm 3.3\%$ under hyperemic conditions. This measurement can serve as an alternative measure of microvascular function and warrants further assessment with murine disease models.

A notable limitation of our current study is that though we were able to image dozens of mice to validate tissue recovery coefficient and to establish K1 measurements, we had limited numbers of mice for certain experiments, including for IMBV measurements (orthogonal experiments each with $n = 3$) and microsphere perfusion experiments ($n = 4$). The low number of mice for microsphere experiments in particular resulted in high variability in resting MBF. Though this does provide constraints for the relationship between K1 and MBF in mice, the uncertainty on these measurements is large. In addition to low numbers, another potential reason for this is the use of a left ventricular injection of the microspheres. One-compartment mixing has been validated in larger animals, but this has not been established in mice.²⁸ Given the small relative size of the left ventricle in mice, two-compartment mixing obtained by injecting microspheres into the left atrium may provide more accurate results. An additional limitation is that the mixing matrix parameters determined in our study are specific to the U-SPECT system which offers high sensitivity and resolution. Though the mixing matrix framework is applicable to other systems, the mixing coefficients would need to be determined for each different model of μ SPECT camera and collimation and may also depend on the reconstruction algorithm and parameters. Lastly, the blood flow and IMBV values are global LV values. These methods could potentially be used to investigate regional microvascular flow and future studies are needed to determine the regional resolution of μ SPECT for this purpose. Thus, to further develop quantitative functional imaging of the coronary microvasculature, future studies are needed to evaluate other tracers with higher extraction fraction at high MBF and to determine the sensitivity of μ SPECT in mouse models of CMVD.

NEW KNOWLEDGE GAINED

Our studies are the first to demonstrate the development and feasibility of dynamic cardiac imaging in mice using a μ SPECT system. We show that we are able to consistently measure left ventricular myocardial activity with imaging and that imaging assumptions that have traditionally been used for large animals do not apply at the scale of the mouse. We also use perfusion microsphere experiments to constrain the relationship between K_1 obtained by imaging and MBF. Lastly, we develop IMBV imaging in mice as an alternative measure of microvascular function.

Acknowledgments

We would like to acknowledge the Penn Cardiovascular Institute Mouse Physiology core for microsphere experiments. Research reported in this publication was supported by the National Center for Advancing Translational Sciences of the National Institutes of Health under Award Number UL1TR001878 and Institute for Translational Medicine and Therapeutics' Transdisciplinary Program in Translational Medicine and Therapeutics. The content is solely the responsibility of the authors and does not necessarily represent the official views of the NIH. MG was supported by K08HL136890. LCJ was supported by T32HL007954.

Disclosure

M. A. Guerraty, L. C. Johnson, E. Blankemeyer, D. J. Rader, S. C. Moore, and S. D. Metzler report no relevant disclosures.

References

1. Camici PG, Crea F. Coronary microvascular dysfunction. *N Engl J Med* 2007;356:830-40.
2. Crea F, Camici PG, Bairey Merz CN. Coronary microvascular dysfunction: an update. *Eur Heart J* 2014;35:1101-11.
3. Bairey Merz CN, Shaw LJ, Reis SE, Bittner V, Kelsey SF, Olson M, et al. Insights from the NHLBI-Sponsored Women's Ischemia Syndrome Evaluation (WISE) Study: Part II: gender differences in presentation, diagnosis, and outcome with regard to gender-based pathophysiology of atherosclerosis and macrovascular and microvascular coronary disease. *J Am Coll Cardiol* 2006;47:S21-9.
4. Murthy VL, Naya M, Taqueti VR, Foster CR, Gaber M, Hainer J, et al. Effects of sex on coronary microvascular dysfunction and cardiac outcomes. *Circulation* 2014;129:2518-27.
5. Gibson CM, Cannon CP, Daley WL, Dodge JT Jr, Alexander B Jr, Marble SJ, et al. TIMI frame count: a quantitative method of assessing coronary artery flow. *Circulation* 1996;93:879-88.
6. Schiattarella GG, Altamirano F, Tong D, French KM, Villalobos E, Kim SY, et al. Nitrosative stress drives heart failure with preserved ejection fraction. *Nature* 2019;568:351-6.
7. Mohammed SF, Hussain S, Mirzoyev SA, Edwards WD, Malieszewski JJ, Redfield MM. Coronary microvascular rarefaction and myocardial fibrosis in heart failure with preserved ejection fraction. *Circulation* 2015;131:550-9.
8. Bairey Merz CN, Pepine CJ, Walsh MN, Fleg JL. Ischemia and no obstructive coronary artery disease (INOCA): Developing evidence-based therapies and research agenda for the next decade. *Circulation* 2017;135:1075-92.
9. Murthy VL, Bateman TM, Beanlands RS, Berman DS, Borges-Neto S, Chareonthaitawee P, et al. Clinical quantification of myocardial blood flow using PET: Joint position paper of the SNMMI cardiovascular council and the ASNC. *J Nucl Cardiol* 2018;25:269-97.
10. Singh P, Schimenti JC, Bolcun-Filas E. A mouse geneticist's practical guide to CRISPR applications. *Genetics* 2015;199:1-15.
11. Zhang H, Qiao H, Frank RS, Huang B, Propert KJ, Margulies S, et al. Spin-labeling magnetic resonance imaging detects increased myocardial blood flow after endothelial cell transplantation in the infarcted heart. *Circ Cardiovasc Imaging* 2012;5:210-7.
12. Raheer MJ, Thibault H, Poh KK, Liu R, Halpern EF, Derumeaux G, et al. In vivo characterization of murine myocardial perfusion with myocardial contrast echocardiography: Validation and application in nitric oxide synthase 3 deficient mice. *Circulation* 2007;116:1250-7.
13. Croteau E, Renaud JM, McDonald M, Klein R, DaSilva JN, Beanlands RS, et al. Test-retest repeatability of myocardial blood flow and infarct size using (1)(1)C-acetate micro-PET imaging in mice. *Eur J Nucl Med Mol Imaging* 2015;42:1589-600.
14. Feher A, Sinusas AJ. Quantitative assessment of coronary microvascular function dynamic single-photon emission computed tomography, positron emission tomography, ultrasound, computed tomography, and magnetic resonance imaging. *Circulation* 2017;10:e006427.
15. Mohy-Ud-Din H, Boutagy NE, Stendahl JC, Zhuang ZW, Sinusas AJ, Liu C. Quantification of intramyocardial blood volume with (99 m)Tc-RBC SPECT-CT imaging: A preclinical study. *J Nucl Cardiol* 2018;25:2096-111.
16. Klein R, Beanlands RSB, deKemp RA. Quantification of myocardial blood flow and flow reserve: Technical aspects. *J Nucl Cardiol* 2010;17:555-70.
17. van der Have F, Vastenhout B, Ramakers RM, Branderhorst W, Krah JO, Ji C, et al. U-SPECT-II: An ultra-high-resolution device for molecular small-animal imaging. *J Nucl Med* 2009;50:599-605.
18. Johnson LC, Guerraty MA, Moore SC, Metzler SD. Quantification of myocardial uptake rate constants in dynamic small-animal SPECT using a cardiac phantom. *Phys Med Biol* 2019;64:065018.
19. Kober F, Iltis I, Cozzone PJ, Bernard M. Myocardial blood flow mapping in mice using high-resolution spin labeling magnetic resonance imaging: Influence of ketamine/xylazine and isoflurane anesthesia. *Magn Reson Med* 2005;53:601-6.
20. Motulsky HJ, Brown RE. Detecting outliers when fitting data with nonlinear regression: A new method based on robust nonlinear regression and the false discovery rate. *BMC Bioinform* 2006;7:123.
21. Renkin EM. Transport of potassium-42 from blood to tissue in isolated mammalian skeletal muscles. *Am J Physiol* 1959;197:1205-10.
22. Crone C. The permeability of capillaries in various organs as determined by use of the 'indicator diffusion' method. *Acta Physiol Scand* 1963;58:292-305.
23. Leppo JA, Meerdink DJ. Comparison of the myocardial uptake of a technetium-labeled isonitrite analogue and thallium. *Circ Res* 1989;65:632-9.
24. Camacho P, Fan H, Liu Z, He JQ. Small mammalian animal models of heart disease. *Am J Cardiovasc Dis* 2016;6:70-80.

25. Sheikine Y, Berman DS, Di Carli MF. Technetium-99 m-sestamibi redistribution after exercise stress test identified by a novel cardiac gamma camera: Two case reports. *Clin Cardiol* 2010;33:E39-45.
26. Sinusas AJ, Bergin JD, Edwards NC, Watson DD, Ruiz M, Makuch RW, et al. Redistribution of 99mTc-sestamibi and 201Tl in the presence of a severe coronary artery stenosis. *Circulation* 1994;89:2332-41.
27. Mousa SA, Cooney JM, Williams SJ. Relationship between regional myocardial blood flow and the distribution of 99mTc-sestamibi in the presence of total coronary artery occlusion. *Am Heart J* 1990;119:842-7.
28. Buckberg GD, Luck JC, Payne DB, Hoffman JI, Archie JP, Fixler DE. Some sources of error in measuring regional blood flow with radioactive microspheres. *J Appl Physiol* 1971;31:598-604.

Publisher's Note Springer Nature remains neutral with regard to jurisdictional claims in published maps and institutional affiliations.